Available online at www.sciencedirect.com
ScienceDirect
International Journal of Heat and Fluid Flow 28 (2007) 1049–1059
International Journal of HEAT AND FLUID FLOW
www.elsevier.com/locate/ijhff

Flow pattern based two-phase frictional pressure drop model for horizontal tubes. Part I: Diabatic and adiabatic experimental study

Jesús Moreno Quibén, John R. Thome *

Laboratory of Heat and Mass Transfer (LTCM), Faculty of Engineering Science (STI) École Polytechnique Fédérale de Lausanne (EPFL), CH-1015 Lausanne, Switzerland

Received 17 March 2006; received in revised form 10 January 2007; accepted 10 January 2007
Available online 17 April 2007

Abstract

The reliable prediction of pressure drop in two-phase flow is an important prerequisite to accurate optimization of thermal systems. Because of the complexity of these types of flow, empirical or semiempirical relationships are only of limited reliability and pressure drops predicted using leading methods often differ by 50% or more. In response to this situation, this work presents an experimental (Part I) and analytical (Part II) investigation of two-phase pressure drops during evaporation in horizontal tubes. The goal of the experimental part was to obtain accurate two-phase pressure drop data over a wide range of experimental conditions. The experimental conditions were chosen so that the effect of the principal parameters could be identified. The range of experimental conditions covered were: three refrigerants (low, medium and high pressure, respectively), two internal tube diameters, eight mass velocities and four heat fluxes (plus adiabatic flow). In addition, using water as the heating fluid, it was possible to cover the entire range of vapor quality. The two-zone test sections allowed tests to (i) be run under both diabatic and adiabatic conditions simultaneously, (ii) to obtain two-phase pressure drop values for nearly every flow regime, and (iii) to validate the data reduction procedure used to obtain the frictional component of the pressure drop. The campaign acquired 2543 experimental two-phase pressure drop values covering five flow regimes.

Keywords: Two-phase flow; Two-phase pressure drops; Flow pattern maps; Flow regimes

1. Introduction

Processes associated with phase-change phenomena are among the most complex transport processes encountered in engineering applications. These processes include all the complexity of single-phase convective transport and additional problems resulting from the motion and deformation of the vapor–liquid interface. Two-phase flow of gases and liquids or vapors and liquids in pipes, channels, equipment, etc. is frequently encountered in industry and has been studied intensively for many years. The reliable prediction of pressure drop in two-phase flows is thereby an important aim; yet, pressure gradients predicted using leading methods often differ by more than 50% according to Ould-Didi et al. (2002) and Moreno Quibén and Thome (2003). Hence, increasingly, attempts are being made to develop prediction methods which are based on phenomenological models and which can be corrected with a minimum of empirical constants using the measured results. The mathematical complexity is kept as low as possible in order to remain practical.

Kattan et al. (1998a,b,c) proposed a physically based (using a simplified interfacial two-phase structure) flow pattern oriented model to predict heat transfer coefficients during evaporation in horizontal tubes. The new heat transfer model was a significant step ahead, improving greatly the predictive accuracy. In addition, in the previously mentioned study by Ould-Didi et al., it was shown that classifying the flow by local flow pattern and then using the best two-phase pressure drop prediction method

* Corresponding author. Tel.: +41 21 693 54 41; fax: +41 21 693 59 60.
E-mail addresses: jesus.moreno@epfl.ch (J. Moreno Quibén), john.thome@epfl.ch (J.R. Thome).

0142-727X/$ - see front matter © 2007 Elsevier Inc. All rights reserved.
doi:10.1016/j.ijheatfluidflow.2007.01.003

for that particular flow pattern resulted in a significant improvement in accuracy. Based on that, the idea now is to extend this physically based approach to the development of a two-phase pressure drop prediction method. Hence, an extensive experimental and analytical study was undertaken. The main experimental objective of this study was to accurately measure two-phase pressure drops over a wide range of experimental conditions to cover the different flow regimes. The analytical objective of this study (in Part II) was then the development of a flow pattern based pressure drop model that respects the two-phase flow structure of the various flow regimes as much as possible while maintaining a degree of simplicity.

2. Flow pattern maps

The analysis of single-phase flow is made easier if one can establish that the flow is either laminar or turbulent and whether any separation or secondary flow effect occurs. This information is equally important in the study of two-phase flow. However, of greater importance in the latter case is the topology or geometry of the flow, i.e. the corresponding flow patterns or flow regimes. To predict the local flow pattern in a tube, a flow pattern map is used. These are an attempt, on a two-dimensional graph, to separate the space into areas corresponding to the various flow regimes. Many flow pattern maps are available for predicting adiabatic two-phase flow regimes in horizontal tubes, such as Baker (1954), Taitel and Dukler (1976), Hashizume (1983) and Steiner (1993). Most of them were developed for adiabatic conditions and then extrapolated to diabatic flow, so the extrapolation procedure may not always produce reliable results. It is desirable to define a flow pattern map that includes the influences of heat flux and dryout on the flow pattern transition boundaries and that is also easy to implement in incremental heat exchanger design schemes. As a first step in this direction, Kattan et al. (1998a) proposed a modification of the Steiner map, which in turn is a modified Taitel–Dukler map, and which includes a method for predicting the onset of dryout at the top of the tube in diabatic annular flow. This map's transitions equations are conveniently presented in coordinates of mass velocity versus vapor quality (G versus x) that facilitates observation of the evolution of flow pattern transitions at fixed mass velocities with increasing vapor quality along an evaporator tube. An improved version of this map was proposed by Zürcher et al. (2002). This improved version of the Kattan flow map respects their ammonia flow pattern observations but is in fact quite complex to implement. To overcome this, an easier to implement version was proposed by Thome and el Hajal (2002). Finally, based on information obtained from dynamic void fraction measurements and observations of the cross-sectional locus of the liquid–vapor interface, a more recent version of the Kattan et al. flow map has been proposed by Wojtan et al. (2005), and also includes an improved method for the effect of heat flux on the transition to mist flow. This new map is illustrated in Fig. 1 where S = stratified flow, SW = stratified-wavy flow, I = intermittent flow, A = annular flow, M = mist flow and D represents the transition zone between annular and mist flow. In the zone indicated as Slug + SW, both these regimes are observed as the flow tends to cycle between one another.

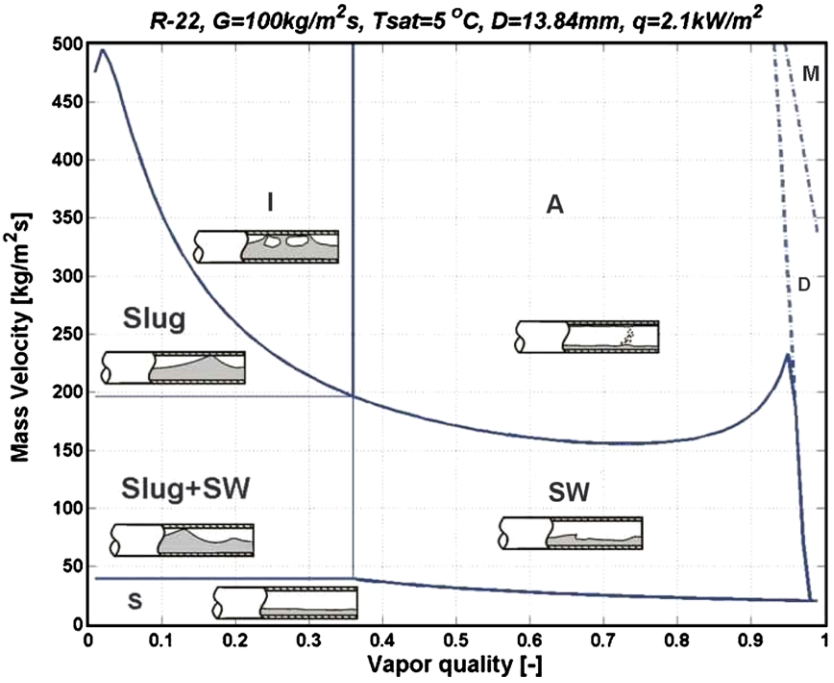

Fig. 1. Flow pattern map evaluated for R-22 at $T_{sat} = 5$ °C in a 13.84 mm internal diameter tube for $q = 2.1$ kW/m^2 using $G = 100$ kg/m^2 s to calculate the void fractions.

This updated version provides a more accurate prediction of different flow regimes (in particular the onset and completion of dryout around the tube perimeter) and does not require any iterative calculations. Therefore, it can be easily used for flow regime identification and, consequently, has been chosen as a starting point for development of the new phenomenological model (Part II). In the interest of conciseness, the implementation procedure for this updated version is not given here but can found in Wojtan et al. (2005).

3. Description of the experimental test facility and test sections

The objective of the experimental part of this study was to run in-tube evaporation tests over a wide range of experimental conditions in order to obtain accurate values of two-phase pressure drops. The ranges of the experimental conditions are shown in Table 1.

The existing test loop has been adapted to be able to run tests over a wide range of test variables. Two new test sections have also been implemented into the modified test rig. The new configuration uses three different sets of transducers to accurately cover the experimental range of two-phase pressure drops. The test facility consists of a refrigerant circuit and a heating water circuit.

Table 1
Experimental conditions for in-tube evaporation tests

Experimental test conditions	
Test fluids	R134a, R22, R410A
Saturation temperature (T_{sat})	5 °C
Internal diameter (D)	8.00, 13.8 mm
Vapor quality (x)	0–1.0
Mass velocity (G)	70–700 kg/m^2 s
Heat flux (q)	6.0–57.5 kW/m^2

3.1. Refrigerant circuit

A schematic of the refrigerant circuit is depicted in Fig. 2. The refrigerant passes first through a series of electrical preheaters and then through an insulated tube before it enters the two-zone test section. In the first zone (called diabatic zone), refrigerant is heated by a counter-current flow of hot water in the annulus of the double pipe system. Then, the refrigerant passes through a visualization zone and through the second part of the test section (called adiabatic zone) where no heat is added or removed from the refrigerant. The refrigerant exits the test section and goes through a condenser, a magnetically driven gear type pump and finally one of two Coriolis mass flow meters. The refrigerant circuit also includes a vapor–liquid reservoir for controlling the amount of refrigerant circulating in the test rig and thus the operating pressure.

3.2. Hot water circuit

The hot water circuit reheats the water after it passes through the diabatic zone of the two-zone test section. The hot water flows counter currently to the refrigerant in the annulus of the test section. The water flow rate is measured by a Coriolis flow meter and the water is circulated by a stainless steel pump. The inlet water temperature is controlled by two secondary water circuits using two plate heat exchangers connected to an industrial cold water circuit. To insure the mixing of the heating water in the

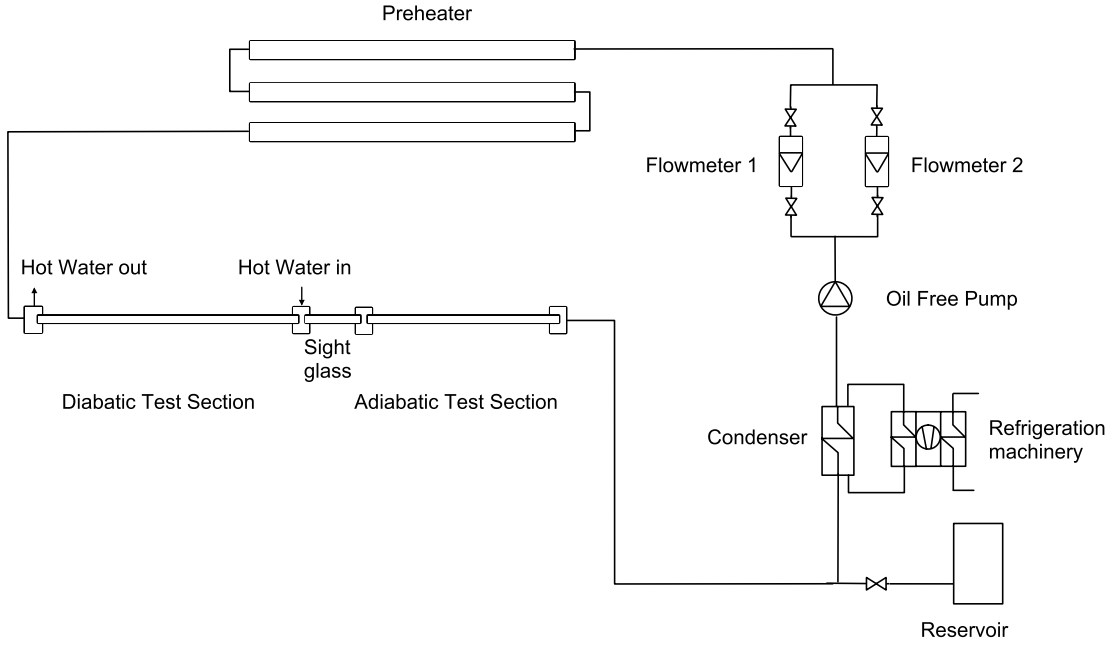

Fig. 2. Schematic of the refrigerant circuit.

annular chamber Reynolds number of the water was always higher than 4500 for the experimental conditions described in Table 1.

3.3. Test sections

Two test sections have been constructed and implemented into the modified test rig. A schematic of the two-zone test section is depicted in Fig. 3. Refrigerant flows into the internal tube from left to right while hot water flows counter-currently into the annulus from right to left.

Both test sections were made of copper and have plain smooth interiors. Internal diameters were 8.00 mm (TS1) and 13.8 mm (TS2), respectively. The outer stainless steel annulus has an internal diameter of 14.00 mm for TS1 and 20.00 mm for TS2. The internal tubes (only diabatic zone) are centered within the outer annulus tube in five positions using centering screws. The external surfaces of both zones of the test section were heavily insulated. The main physical properties and geometrical dimensions of the test sections are shown in Table 2, where D is the internal diameter of the tube, D_{ext} is the external diameter of the tube, z_{diab} is the length of the diabatic zone, z_{adiab} is the length of the adiabatic zone, λ is the thermal conductivity and δ_{wat} is the annular gap for the heating water in the diabatic zone.

3.4. Experimental procedure and data acquisition

All the measurements were made with a computer equipped with a National Instruments SCXI data acquisition system. In order to measure a test parameter in a channel, 100 acquisitions were made in 0.02 s (50 Hz electrical period) and the average of these 100 values was calculated during the acquisition. The result is the measured value of the channel. By this way, any noise from alternating current on the measured signal is removed. This value is stored and the system goes to the next channel. With this measurement method, the theoretical channel measurement frequency is 50 channels per second, but due to the switching time between channels, the actual frequency is 30 channels per second. In total, it takes 4.3 s to measure all the channels of the acquisition system once. To obtain one experimental point, 10 of such acquisition cycles are recorded and averaged.

3.5. Measurements

The major objective of the experimental part of this work was to measure two-phase pressure drops over the vapor quality range from 0 to 1. Two-phase pressure drop values were directly obtained from the differential pressure transducers. Meanwhile to completely establish the experi-

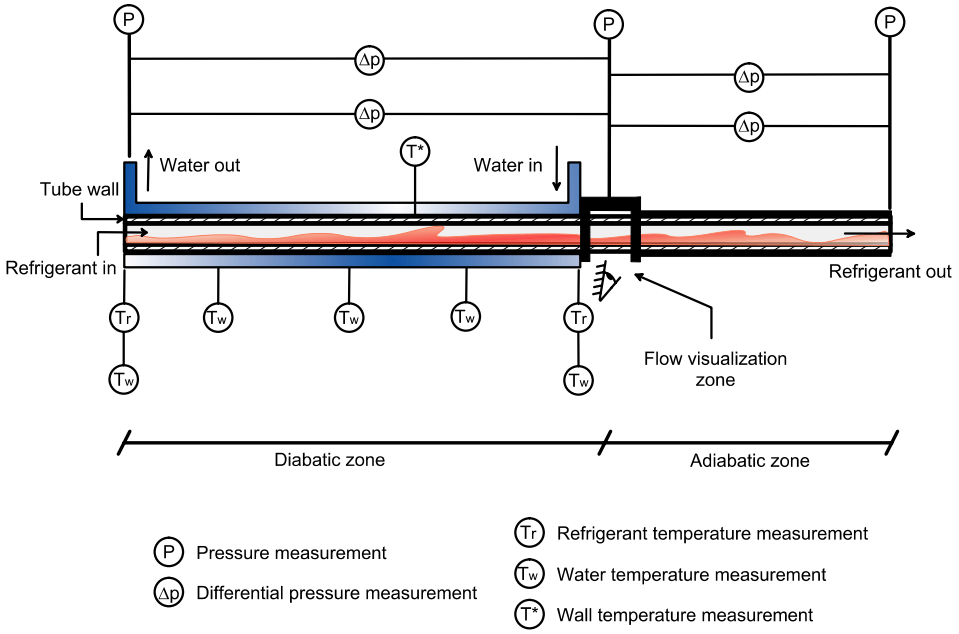

Fig. 3. New two-zone test section.

Table 2
Main properties and geometrical dimensions of the implemented test sections

	Internal tube						External tube			
	Mat.	D_{ext} (mm)	D (mm)	z_{diab} (mm)	z_{adiab} (mm)	λ (W/m K)	Mat.	D_{ext} (mm)	D (mm)	δ_{wat} (mm)
TS1	Cu	9.53	8.00	2035	980	339	SS	17.40	14.00	2.235
TS2	Cu	15.87	13.8	2026	989	339	SS	23.00	20.00	2.065

mental conditions, some others parameters need to be determined by calculation from measured values.

3.5.1. Pressure drop

The two-phase pressure drops across the diabatic test sections were each measured by a selection of sensors depending on the level of the pressure drop being measured. For the diabatic test section, two differential pressure transducers (0–40 mbar and 0–500 mbar) were used for the small and intermediate pressure drops and a pair of absolute pressure sensors (0–25 bar) for pressure drops larger than 500 mbar. For the adiabatic test section, two differential pressure transducers (0–20 and 0–160 mbar) were used plus a similar pair of absolute pressure sensors.

3.5.2. Refrigerant temperature

The saturation temperature of the refrigerant T_{sat} was calculated using the pressure measurements at the inlet and outlet of the diabatic part of the test section. Then, knowing the saturation pressure P_{sat}, the saturation temperature is obtained based on the thermodynamical properties calculated using REFPROP (1998).

3.5.3. Heat flux

Heat is transferred from the hot water to the refrigerant. The temperature of the water is measured at five positions (represented as T_w in Fig. 3) with a total of 26 thermocouples giving five local water temperature values T_w. The enthalpy of the flowing water is given by the following equation:

$$h_w = c_{p_{water}} T_w \tag{1}$$

From Eq. (1), five discrete enthalpy values were obtained from the five water temperature measurement points. These points were used to determine the enthalpy profile over the diabatic test section. For the enthalpy profile determination, a second order polynomial fit has been used. Then, the heat transferred from the water between two points of the test section can be defined as:

$$Q_{12} = (h_{w2} - h_{w1})\dot{M}_w \tag{2}$$

The derivative of Eq. (2) with respect to axial position along the tube divided by the tube perimeter gives the external heat flux q_{ext} along an elementary length dz:

$$q_{ext} = \frac{1}{\pi D_{ext}} \frac{dQ}{dz} = \frac{\dot{M}_{wat}}{\pi D_{ext}} \left(\frac{dh_w(z)}{dz} \right) \tag{3}$$

Thus, knowing the enthalpy profile $h_w(z)$, the external heat flux can be calculated at any point along the diabatic test section. The internal heat flux provided to the refrigerant is determined as:

$$q(z) = q_{ext} \left(\frac{D_{ext}}{D} \right) = \frac{\dot{M}_w}{\pi D} \left(\frac{dh_w(z)}{dz} \right) \tag{4}$$

3.5.4. Vapor quality

The vapor quality is calculated by an energy balance over the preheater and the test section. Hence, the vapor at any test section position can be calculated fom the following equation:

$$x(z) = \frac{P + \dot{M}_w c_w \left(T_{w(inlet)} - T_w(z) \right)}{\dot{M}_{ref} h_{LV}} \tag{5}$$

where P is the electrical power provided by the preheater, $T_{w(inlet)}$ is the temperature of the heating water at the refrigerant's inlet to the diabatic test section, $T_w(z)$ is the water temperature at any position along the test section, c_w is the water specific heat, and $\dot{M}_w$ and $\dot{M}_{ref}$ are the water and refrigerant mass flow rates, respectively.

3.6. Accuracy of measurements

3.6.1. Energy balances

Liquid–liquid tests have been done with subcooled R22 and R410A versus water for both test sections. The accuracy of the energy balance between the heating and cooling fluids was thus determined. The results of these tests showed that Q_w/Q_{ref} varied from 0.98 to 1.02, with a mean error of ±0.98% for R410A and ±0.96% for R22 in the 13.8 mm test section. Similar results were obtained for the 8 mm test section. This is very accurate for this type of measurement and confirms that all precisely calibrated measurement instruments were working correctly.

3.6.2. Pressure drop measurement accuracy

Two different types of pressure transducers were used to measure the two-phase pressure drops, namely, absolute and differential. The pair of absolute transducers used in this study ranged 1–25 bar. They were calibrated with a very accurate balance and their accuracy was found to be ±20 mbar within the pressure range of the tests. Four differential transducers were used for the small and intermediate range in this study. They ranged 0–20 mbar and 0–40 mbar for the low range and 0–160 mbar and 0–500 mbar for the intermediate. An accuracy of ±0.05% F.S. was given by the supplier. After inhouse calibration against a water column, this value was found to be realistic and taken as the accuracy of the transducers.

3.6.3. Heat flux measurement accuracy

The absolute error of the heat flux Δq can be determined with the following expression obtained from Eq. (4):

$$\Delta q(z) = \sqrt{\left(\frac{dq(z)}{d\dot{M}_w} \Delta \dot{M}_w \right)^2 + \left(\frac{dq(z)}{dT_w} \Delta T_w \right)^2} \tag{6}$$

After calculation, the mean relative error does not exceed 2% and 1% for the 13.8 mm and 8 mm test sections, respectively.

3.6.4. Vapor quality measurement accuracy

Assuming that all measured values are linearly independent, the absolute vapor quality error applied to Eq. (5) can be expressed as:

$$\Delta x(z)=\sqrt{\left(\frac{\partial x}{\partial P}\Delta P\right)^2+\left(\frac{\partial x}{\partial T1_{\text{water}}}\Delta T1_{\text{water}}\right)^2+\left(\frac{\partial x}{\partial T_{\text{wat}}(z)}\Delta T_{\text{wat}}(z)\right)^2+\left(\frac{\partial x}{\partial \dot{M}_{\text{wat}}}\Delta \dot{M}_{\text{wat}}\right)^2+\left(\frac{\partial x}{\partial \dot{M}_{\text{ref}}}\Delta \dot{M}_{\text{ref}}\right)^2+\left(\frac{\partial x}{\partial P_{\text{sat}}}\Delta P_{\text{sat}}\right)^2} \tag{7}$$

The term with the saturation pressure P_{sat} in the vapor quality error calculation is encountered because the latent heat of the refrigerant is determined from the measurement of the saturation pressure.

The absolute uncertainty for the heating power measurements is ±20 W and the relative accuracy of the temperature measurements is ±0.02 °C. The absolute error of the absolute pressure transducers after calibration has been estimated to be ±20 mbar. The refrigerant and water mass flow rates are measured with an accuracy of ±0.15%. After calculating of partial derivatives and substituting all values in Eq. (7), the maximum absolute errors for each tested mass velocity have been obtained. The calculated mean relative errors do not exceed 2% and 3% for the 13.8 mm and 8 mm test sections, respectively.

4. Reduction of experimental data

The general expression for describing the total two-phase pressure drop Δp_{total} is:

$$\Delta p_{\text{total}}=\Delta p_{\text{static}}+\Delta p_{\text{mom}}+\Delta p_{\text{frict}} \tag{8}$$

where Δp_{static} is the elevation head pressure drop (presently $\Delta p_{\text{total}}=0$ for a horizontal tube), Δp_{mom} is the momentum pressure drop created by acceleration of the flow in a diabatic process and Δp_{frict} is the two-phase frictional pressure drop.

The two-zone test sections yields the two-phase pressure drops in the diabatic (first zone) and adiabatic (second zone) simultaneously. The adiabatic two-phase pressure drops were obtained at the vapor quality leaving the diabatic test section and for the reason mention above (adiabatic process) the momentum pressure drop $\Delta p_{\text{mom}}=0$. Hence, one can directly determine the two-phase frictional pressure drops in the adiabatic test section from the measured values:

$$\Delta p_{\text{frict}}=\Delta p_{\text{total}} \tag{9}$$

For the diabatic test section one determines the two-phase frictional pressure drops from the following equation:

$$\Delta p_{\text{frict}}=\Delta p_{\text{total}}-\Delta p_{\text{mom}} \tag{10}$$

Hence, one must first evaluate the momentum pressure drop Δp_{mom} to obtain the frictional pressure drop values. The momentum pressure drop in the diabatic test section is given by the following expression:

$$\Delta p_{\text{mom}}=G^2\left\{\left[\frac{(1-x)^2}{\rho_{\text{L}}(1-\epsilon)}+\frac{x^2}{\rho_{\text{G}}\epsilon}\right]_{\text{out}}-\left[\frac{(1-x)^2}{\rho_{\text{L}}(1-\epsilon)}+\frac{x^2}{\rho_{\text{G}}\epsilon}\right]_{\text{in}}\right\} \tag{11}$$

where G is the total mass velocity of liquid plus vapor, x is the vapor quality at the inlet or outlet of the test section, ϵ is the vapor cross-sectional void fraction at the inlet or outlet of the test section, ρ_{L} and ρ_{V} are the liquid and vapor densities and g is 9.81 m/s^2. Based on the recent work by Wojtan et al. (2004), they found the Steiner (1993) version of the Rouhani and Axelsson (1970) drift flux model to be very accurate for predicting void fractions in similar experimental conditions:

$$\epsilon=\frac{x}{\rho_{\text{G}}}\left[(1+0.12(1-x))\left(\frac{x}{\rho_{\text{G}}}+\frac{(1-x)}{\rho_{\text{L}}}\right)+\frac{1.18(1-x)[g\sigma(\rho_{\text{L}}-\rho_{\text{G}})]^{0.25}}{G\rho_{\text{L}}^{0.5}}\right]^{-1} \tag{12}$$

This expression is used in Eq. (11) to determine the momentum pressure from the experimental conditions.

Using water in the annulus of the double pipe system to evaporate the refrigerant, the water undergoes a temperature change while the phase changing refrigerant stays at nearly the same saturation temperature. This causes a change in the local heat flux as the temperature difference between the water and the refrigerant decreases during the evaporation process along the length of the tube. In order to determine the momentum pressure drop created by acceleration of the flow Δp_{mom}, one must known the vapor quality. As this is changing during the evaporation process, the results are reported at the mean vapor quality in the diabatic test section based on an evaluation (piecewise decomposition) of the enthalpy profile obtained from the water-side.

Fig. 4 shows the total, momentum and frictional pressure drops for a representative set of experimental conditions for the 8 mm and 13.8 mm tube, respectively. The momentum pressure drops were calculated following the procedure detailed previously and the total pressure drops correspond to the measured values. As expected, the momentum pressure drop is larger for high heat fluxes

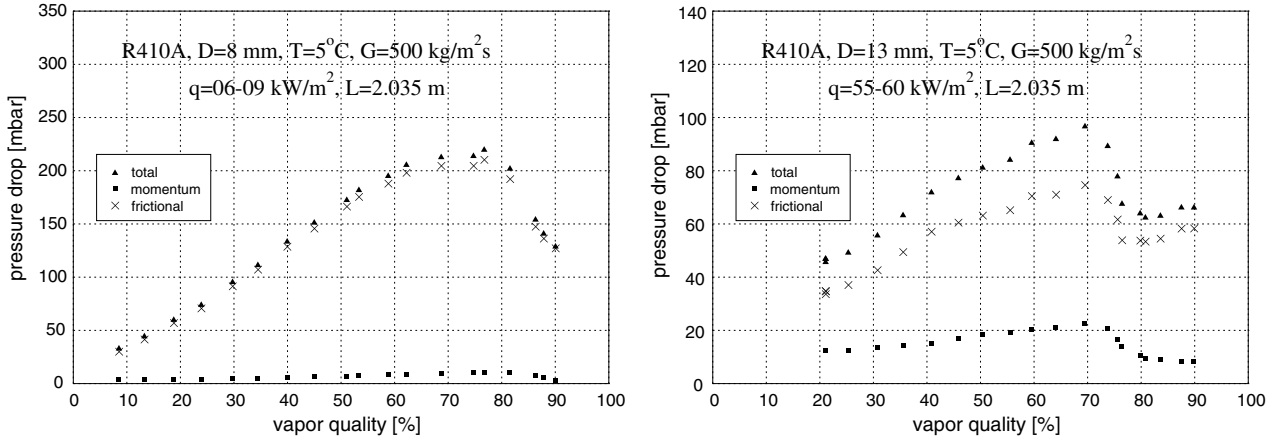

Fig. 4. Total, frictional and momentum pressure drops versus vapor quality at different experimental conditions.

and vary from around 3% of the total pressure drop for the lowest heat fluxes up to 40% for the highest.

5. Experimental frictional pressure drop results

5.1. Adiabatic versus diabatic two-phase pressure gradients

Fig. 5 shows a comparison, for a representative set of experimental conditions, of the two-phase pressure gradients for the adiabatic test section versus those for the diabatic test section. The agreement between the results is quite remarkable, attesting to the accuracy and reliability of the measurements as well as the data reduction procedure. At high vapor qualities, the difference between the two types of measurements is thought to be caused by the vapor quality variation along the diabatic test section around the peak, which averages out the pressure gradient rather than giving the "local" value at a particular vapor

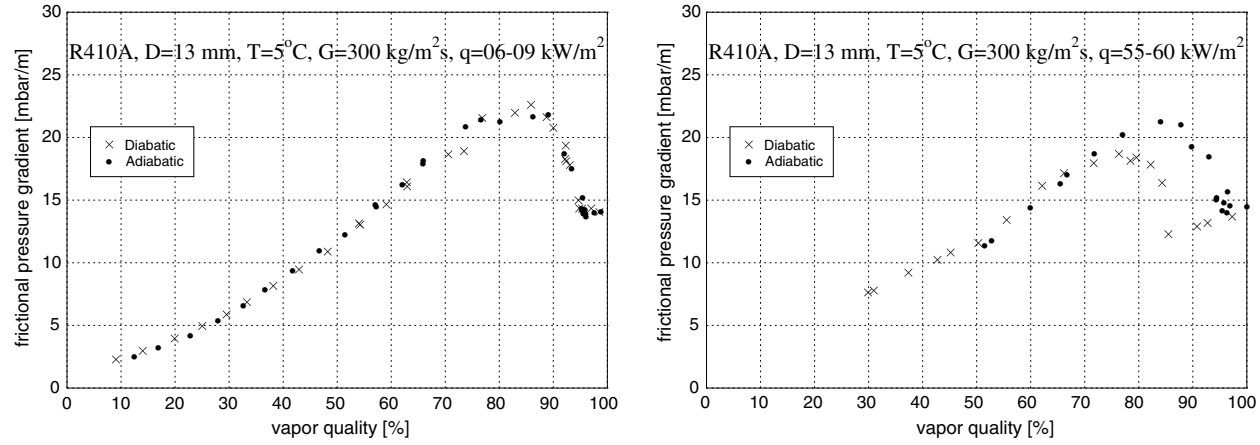

Fig. 5. Adiabatic versus diabatic test section results for R410A.

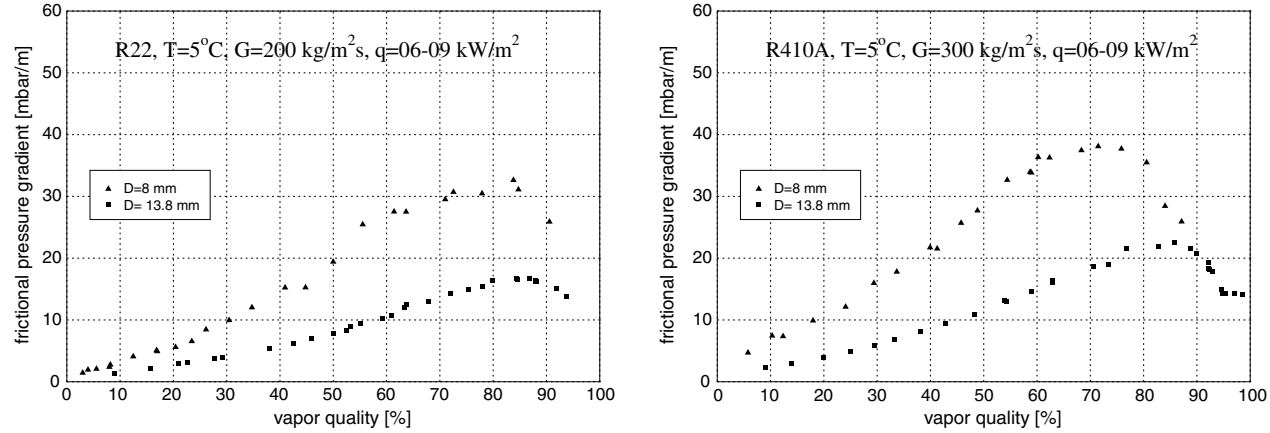

Fig. 6. Frictional pressure gradients versus vapor quality for R22 and R410A.

quality as in the adiabatic test section. For instance, in the diabatic test section at the vapor quality at the peak, part of the test section will be operating at local conditions before the peak and part at local conditions after the peak, resulting in a lower value than for the adiabatic test section at the same vapor quality. It is for this range of test conditions that the adiabatic test section was added to the loop in order to obtain data representative of the real pressure gradients at high vapor qualities near and after the peak.

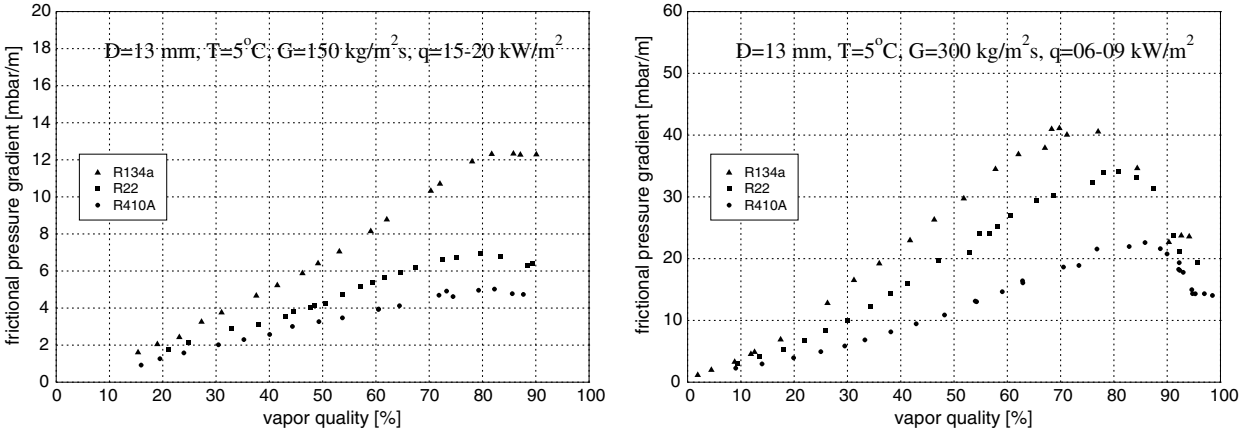

Fig. 7. Comparison of the frictional pressure gradients for R134a, R22 and R410A at two experimental conditions.

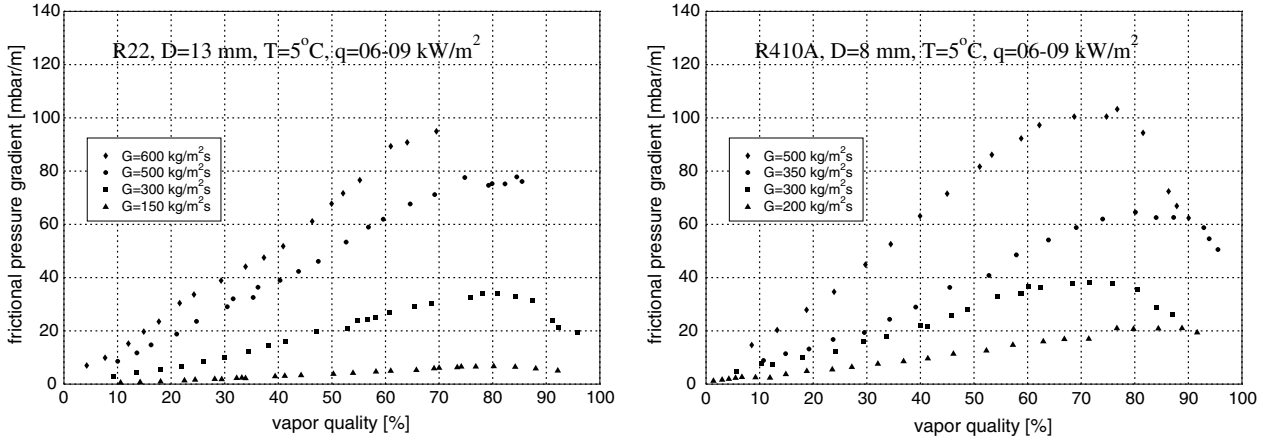

Fig. 8. Frictional pressure gradients versus vapor quality for different mass velocities.

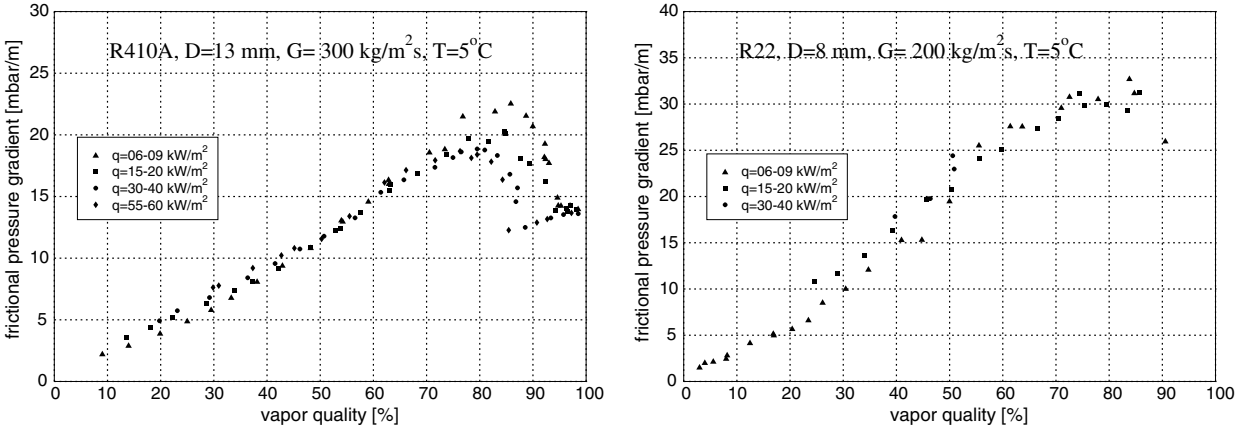

Fig. 9. Frictional pressure gradients versus vapor quality at different heat fluxes.

5.2. Comparisons for different experimental parameters

5.2.1. Diameter

Fig. 6 depicts a comparison of the two-phase frictional pressure drops for the two internal diameters tested at a particular set of test variables. The smaller diameter tube induces a larger two-phase pressure gradient.

5.2.2. Fluid

Fig. 7 shows that the frictional two-phase pressure gradients are largest for R134a and smallest for R410A with R22 in the middle. The data for each fluid shows the characteristic rise in two-phase frictional pressure gradient with rising vapor quality, a peak at high vapor quality, and the subsequent falloff as the vapor quality approaches 100%.

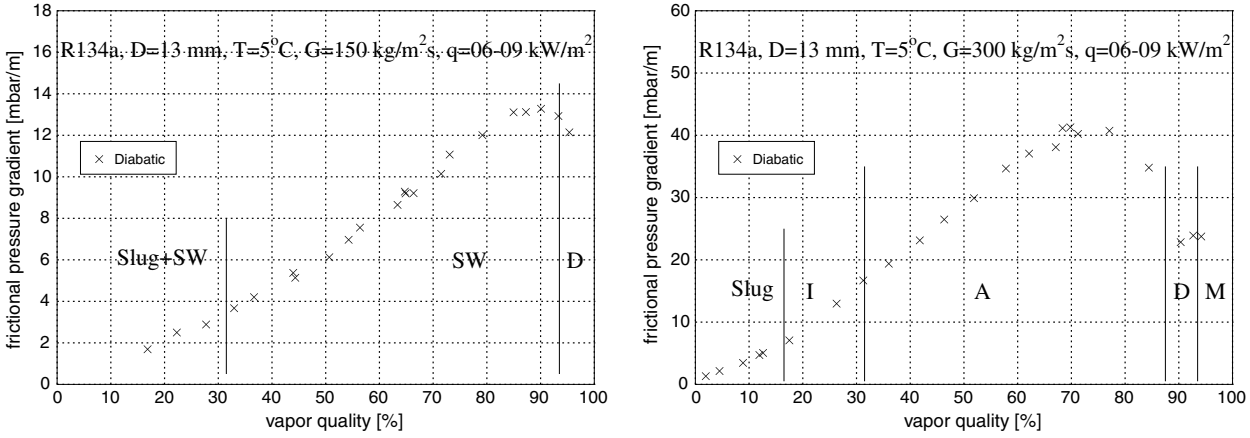

Fig. 10. Frictional pressure gradients versus vapor quality for R134a at different experimental conditions.

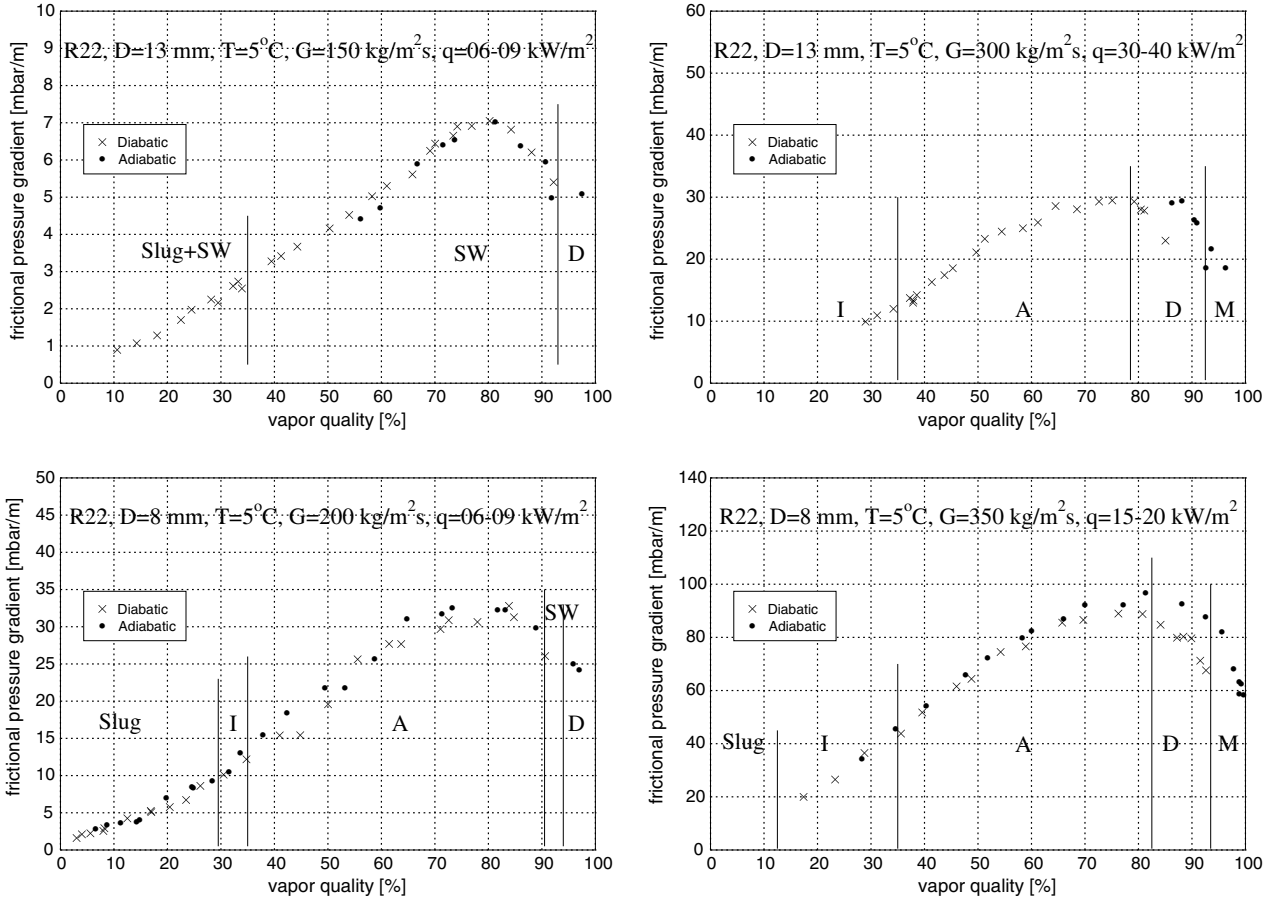

Fig. 11. Frictional pressure gradients versus vapor quality for R22 at different experimental conditions.

The trends in the data are seen to be very clear with little scatter in the data because of the accuracy of the transducers and energy balances and the fine control on the steady-state operating conditions.

5.2.3. Mass velocity

Fig. 8 depicts the experimental results for R22 and R410A at several mass velocities. As expected, the frictional pressure gradient increases with mass velocity.

5.2.4. Heat flux

Fig. 9 illustrates the frictional pressure drop data obtained at different heat fluxes, from rather low to quite high values. The effect of the evaporation heat flux is seen to be of only minor importance at vapor qualities before the peak. At high vapor qualities, the peak is shifted to lower vapor qualities by the increase in the heat flux, representing the most important influence of heat flux on the observations. The location of the peaks is near to the onset of dryout at the top of the tube where the top of the tube is dry after the peak. However, the peaks in the frictional pressure gradients sometimes preceed the analogous peaks in the locally measured heat transfer coefficients. Hence, the peak in pressure gradient can occur before dryout and thus the peak is probably sometimes associated with the damping out of interfacial waves as the annular film thins.

For the highest heat fluxes, based on visual observations in the sight glass at the end of the diabatic test section, the flow was observed to convert to mist flow, and these are the data at high vapor quality that depict an increasing trend with vapor quality after the falloff, e.g. such as those in the left graph at $q = 55$–$60\ \mathrm{kW/m^2}$.

5.3. Results for R134a, R22 and R410A

Figs. 10–12 illustrate the frictional pressure drop data obtained for R134a, R22 and R410A for a representative set of experimental conditions. The complete set of experimental results can be found in Moreno Quibén (2005). For refrigerant R134a, only tests with the 13.8 mm test section were performed and it has to be pointed out that the adiabatic test section was added in the middle of experimental campaign so that only diabatic results are reported in graphs for this fluid. Flow pattern transitions calculated using Wojtan–Ursenbacher–Thome flow pattern map have been added to the graphs as vertical solid lines.

6. Conclusions

As the first step in this work, a comprehensive experimental study was undertaken in order to obtain accurate two-phase pressure drop values during evaporation of

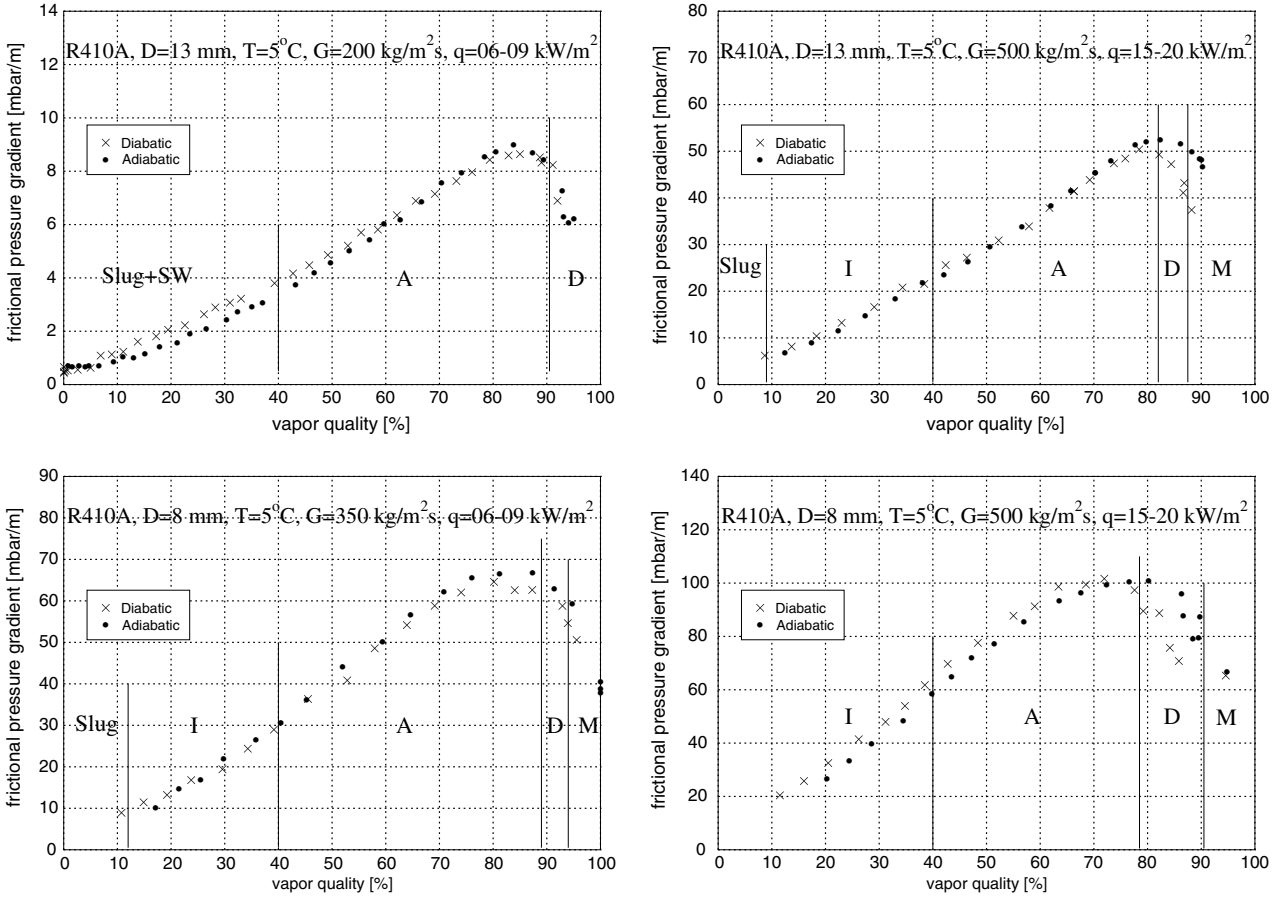

Fig. 12. Frictional pressure gradients versus vapor quality for R410A at different experimental conditions.

refrigerants in horizontal tubes. The experimental conditions were chosen to obtain experimental values over a wide range of test parameters so that the effect of each parameter could be easily identified. The range of experimental conditions covered were: three refrigerants (low, medium and high pressure), two internal tube diameters, eight mass velocities and four heat fluxes, covering the entire range of vapor quality. Fulfilling these experimental requirements imposed a modification of the existing experimental facility and the implementation of new test sections. The new two-zone test sections allowed tests to (i) be run under both diabatic and adiabatic conditions simultaneously, (ii) to obtain two-phase pressure drop values for nearly every flow regime, and (iii) to validate the data reduction procedure used to obtain the frictional component of the pressure drop. The campaign acquired 2543 experimental two-phase pressure drop values covering all flow regimes except bubbly and stratified because of operating limitations.

As a validation of the data reduction procedure, a set of graphs showed comparisons, for a representative set of experimental conditions, of the two-phase frictional pressure gradients for the adiabatic test section versus those for the diabatic test section. The agreement was shown to be quite remarkable attesting to the accuracy and reliability of the measurements as well as the aptness of the data reduction protocol and choice of void fraction model. Afterwards a parametric study to evaluate the influence of the test variables was undertaken. A set of graphs, for a selected representative values of the test variables, showed that while the fluid, diameter and mass velocity had a strong effect over the entire range of vapor quality, the heat flux influenced the measured values only for a particular range of vapor qualities near and after the onset of dryout.

Acknowledgements

The project has been supported financially by the Fond National Swiss (FNS) contract number 21-57210.99 and by the Air-Conditioning and Refrigeration Technology Institute (ARTI) contract number 605-20040, which are gratefully acknowledged.

References

Baker, O., 1954. Design of pipe lines for simultaneous flow of oil and gas. Oil and Gas Journal 53, 185–190.

Hashizume, K., 1983. Flow pattern and void fraction of refrigerant two-phase flow in a horizontal pipe. Bulletin of the JSME 26, 1597–1602.

Kattan, N., Thome, J.R., Favrat, D., 1998a. Flow boiling in horizontal tubes. Part 1 – development of a diabatic two-phase flow pattern map. Journal of Heat Transfer 120, 140–147.

Kattan, N., Thome, J.R., Favrat, D., 1998b. Flow boiling in horizontal tubes. Part 2 – new heat transfer data for five refrigerants. Journal of Heat Transfer 120, 148–155.

Kattan, N., Thome, J.R., Favrat, D., 1998c. Flow boiling in horizontal tubes. Part 3 – development of a new heat transfer model based on flow pattern. Journal of Heat Transfer 120, 156–165.

Moreno Quibén, J., 2005. Experimental and analytical study of two-phase pressure drops during evaporation in horizontal tubes. Thesis No. 3337, Swiss Federal Institute of Technology, Lausanne.

Moreno Quibén, J., Thome, J.R., 2003. Two-phase pressure drops in horizontal tubes: new results for R-410A and R-134a compared to R-22, paper IIC00. In: Proceeding of the 21st IIR International Congress of Refrigeration, Washington, DC, USA.

Ould-Didi, M.B., Kattan, N., Thome, J.R., 2002. Prediction of two-phase pressure gradients of refrigerants in horizontal tubes. International Journal of Refrigeration 25, 935–947.

REFPROP, 1998. Refrigerant Properties Database 23, Version 6.01. NIST, Gaithersburg, MD.

Rouhani, S.Z., Axelsson, E., 1970. Calculation of void volume fraction in the subcooled and quality boiling regions. International Journal of Heat and Mass Transfer 13, 383–393.

Steiner, D., 1993. VDI-Wärmeatlas (VDI Heat Atlas). Verein Deutscher Ingenieure VDI-Gessellschaft Verfahrenstechnik und Chemieingenieurwessen (GCV), Düsseldorf, Ch. Hbb.

Taitel, Y., Dukler, A.E., 1976. A model for predicting flow regime transitions in horizontal and near horizontal gas–liquid flow. AIChE Journal 22, 47–55.

Thome, J.R., el Hajal, J., 2002. Two-phase flow pattern map for evaporation in horizontal tubes: latest version. In: Proceedings of the 1st International Conference on Heat Transfer, Fluid Mechanics and Thermodynamics, Kruger Park, South Africa.

Wojtan, L., Ursenbacher, T., Thome, J.R., 2004. Interfacial measurements in stratified types of flow. Part II: mesurements for R22 and R-410A. International Journal of Multiphase Flow 30, 125–137.

Wojtan, L., Ursenbacher, T., Thome, J.R., 2005. Investigation of flow boiling in horizontal tubes. Part I – a new diabatic two-phase flow pattern map. International Journal of Heat and Mass Transfer 48, 2955–2969.

Zürcher, O., Favrat, D., Thome, J.R., 2002. Development of a adiabatic two-phase flow pattern map for horizontal flow boiling. International Journal of Heat and Mass Transfer 45, 291–301.